Published version available at: https:doi.org/10.1080/13647830.2022.2049370

Flame stabilization by a highly conductive body: multiple steady-state solutions and time-dependent dynamics

Vadim N. Kurdyumov [1], Carmen Jiménez

Department of Energy, CIEMAT, Avda. Complutense 40, 28040 Madrid, Spain

Abstract

We present an investigation of the stabilization of premixed laminar flames by means of an isolated highly conductive bluff-body, a circular cylinder, placed in a uniform flow of a combustible mixture. It is shown that the problem has non-unique steady-state solutions for certain values of the parameters. Moreover, we solve the time-dependent equations to check the stability of the solutions and demonstrate the possibility of controlling the convergence to a certain steady-state solution.

1 Introduction

Stabilization of premixed flames in a flow of a combustible mixture is one of the most important tasks in combustion. Several different configurations have been proposed to attain this effect. One of the most common is the flame stabilization by means of a bluff-body. Despite the fact that the systematic studies of this problem can be traced back more than sixty years [1–5], important aspects remain unexplored to this day.

The use of computational facilities has recently allowed advances in the understanding of flame stabilization processes [6–19]. The predominant configuration for numerical simulations was a body placed in a channel. Most of these investigations were carried out in the framework of two-dimensional models. The effect of solid materials on the blow-off limit of a micro-combustor was investigated in [6]. The influence of the flame holder temperature on the stabilization of a laminar methane flame on a cylinder was presented in [7]. Considerable effort has gone into modeling complex chemical kinetics [8–11,15–17] and conjugate heat transfer [12–17], which implies large computational costs for exhaustive parametric analysis. Premixed flames stabilized behind the trailing edge of a semi-infinite cylindrical rod placed coaxially in a circular channel were investigated in [18] within the framework of a three-dimensional diffusive-thermal model allowing a global linear stability analysis of steady-state solutions.

[1]Corresponding author

A series of experimental and numerical studies of a flame stabilized behind a fixed and a rotating cylinder in [7, 12–14] have shown different flame positions, shapes and dynamics when the temperature of the flame holder is forced to change. In a recent study [19], the flame stabilization by means of a solid square maintained at a constant temperature in a laminar channel flow was studied. In particular, it was found that for certain values of the parameters, multiple steady-state solutions corresponding to a zero value of the total heat flux on the square surface arise. The presence of various geometric parameters when the stabilization problem is formulated in a channel of finite width creates some difficulties for conducting an exhaustive parametric analysis. It is also obvious that in the case of multiple solutions not all of the solutions are stable.

In the present work, the problem of a flame stabilized by means of a circular cylinder placed perpendicularly in a uniform flow is studied applying a number of simplifications. This allows us to focus on the physical reasons for the appearance of non-unique steady-state solutions and to investigate their stability. The article is arranged as follows: in Section 2, the general formulation is given; a description of the numerical treatment is outlined in Section 3; steady-state solutions are presented in Section 4 and the temporal dynamics are studied in Section 5. Finally, conclusions are drawn in the last section. Asymptotic considerations leading to the approximation used in this work are discussed in the Appendix.

2 Mathematical formulation

Let us consider a circular cylinder of radius R placed perpendicularly to an incoming flow of a combustible mixture. The mixture has an initial temperature T_0 and moves with a uniform velocity U_0 far upstream relative to the cylinder. We assume that the planar flame speed, S_L, is less than the velocity of the mixture, $S_L < U_0$, thus preventing the flame to propagate upstream. Under this condition, flame stabilization is only possible under the action of the cylinder that works like a flame holder. The sketch of the problem and the coordinate system are shown in Fig. 1. For simplicity, the problem statement is limited to a two-dimensional consideration and all solutions are assumed to be mirror-symmetric about the x-axis. Thus, all dependent variables are functions of the spatial variables r and φ, where $x = r\cos\varphi$, $y = r\sin\varphi$ and $0 < \varphi < \pi$.

For the sake of simplicity, the mixture is assumed to be deficient in fuel. The mass fraction of fuel, denoted by Y and with the initial value Y_0, is followed. The mass fraction of the oxidizer, which is in abundance, remains nearly constant. The amount of fuel consumed per unit volume

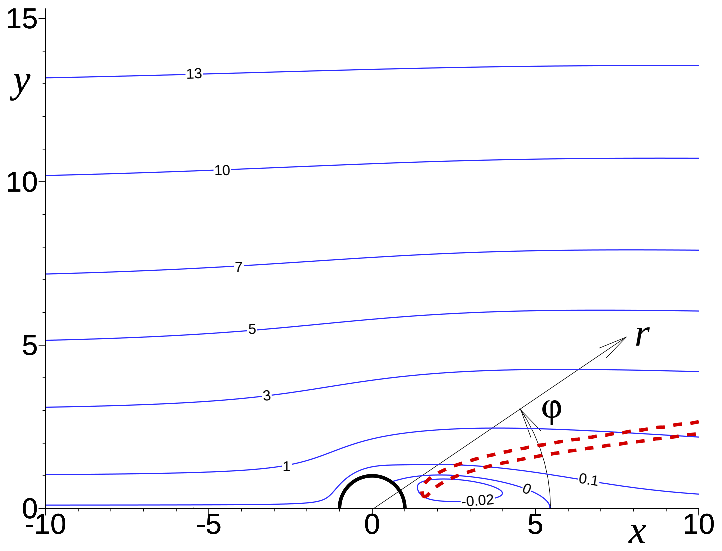

Figure 1: Sketch of the problem, the coordinate system, the illustration of an anchored flame (a dashed-line contour) and stream function isolines (solid lines) calculated for $Re = 20$.

and per unit time is given by $\Omega = \mathcal{B}\rho^2 Y \exp(-E/\mathcal{R}T)$, where $\mathcal{B}$ is a pre-exponential factor, ρ is the density of the mixture, E is the overall activation energy and $\mathcal{R}$ is the universal gas constant.

For the phenomenon studied in this work, the thermal interaction between the flame and the flame holder is fundamental, while the influence of the flame on the gas velocity field seems to be secondary. Thus, the effects associated with thermal expansion will be discussed elsewhere. In the following, we consider a diffusive-thermal model, formally assuming that the density of the mixture ρ, the thermal diffusivity $\mathcal{D}_T$, the individual molecular fuel diffusivity D, the heat capacity c_p, and the kinematic viscosity ν are all constant. Consequently, the flow field is not affected by the combustion field and is determined a priori by solving the standard Navier-Stokes equations. This study is limited to considering rather thin cylinders assuming that the corresponding Reynolds numbers are not large. Thus, the velocity field is assumed to be independent of time. If the characteristic length and speed are chosen as R and U_0 and the pressure variations are made dimensionless using the dynamic pressure ρU_0^2 , the velocity field $\mathbf{v}$ is determined from

$$\begin{aligned} &(\mathbf{v}\cdot\nabla)\mathbf{v} = -\nabla p + Re^{-1}\Delta\mathbf{v}, \quad \nabla\cdot\mathbf{v} = 0, \\ &r = 1: \quad \mathbf{v} = 0, \qquad r \to \infty: \quad \mathbf{v} = \mathbf{e}_x, \end{aligned} \tag{1}$$

where $Re = RU_0/\nu$ is the Reynolds number.

The combustion field is determined by the coupled energy and fuel balance equations with the velocity field computed from Eqs. (1). In the following, the laminar flame speed of the planar adiabatic flame S_L and the thermal flame thickness defined as $\delta_T = \mathcal{D}_T/S_L$ are used to specify the non-dimensional parameters. The non-dimensional temperature is defined by $\theta = (T - T_0)/(T_e - T_0)$, where $T_e = T_0 + QY_0/c_p$ represents the adiabatic temperature of the corresponding planar flame, and the fuel mass fraction is normalized by its upstream value Y_0. Choosing the convection time R/U_0 as a unit of time, the dimensionless transport equations become

$$\frac{\partial \theta}{\partial t} + (\mathbf{v} \cdot \nabla)\theta = \frac{1}{RePr}\,\Delta\theta + \frac{d}{RePr}\,\omega \tag{2}$$

$$\frac{\partial Y}{\partial t} + (\mathbf{v} \cdot \nabla)Y = \frac{1}{LeRePr}\,\Delta Y - \frac{d}{RePr}\,\omega \tag{3}$$

where $\Delta = \partial^2/\partial r^2 + r^{-1}\partial/\partial r + r^{-2}\partial^2/\partial\varphi^2$ is the Laplace operator and

$$\omega = \frac{\beta^2}{2Le\,u_p^2} Y \exp\left\{\frac{\beta(\theta - 1)}{1 + \gamma(\theta - 1)}\right\} \tag{4}$$

is the dimensionless reaction rate.

The following non-dimensional parameters appear in the above equations: the Zel'dovich number, $\beta = E(T_e - T_0)/\mathcal{R}T_e^2$, the Lewis number, $Le = \mathcal{D}_T/\mathcal{D}$, the heat release parameter, $\gamma = (T_e - T_0)/T_e$, the Prandtl number, $Pr = \nu/\mathcal{D}_T$, the Reynolds number, $Re = U_0R/\nu$, and the reduced Damköhler number, $d = R^2/\delta_T^2$. In the calculations reported below, $\beta = 10$, $\gamma = 0.7$, $Le = 1$ and $Pr = 0.72$ were assigned. The influence of these parameters on the effects described below will be reported elsewhere.

The above formulation allows to study the influence of the flow field and chemistry independently. Indeed, for a fixed cylinder radius, changes in the Reynolds number and the Damköhler number can be made separately by varying the velocity of the incident flow, U_0, and the velocity of the planar flame front, S_L, respectively. The latter can be accomplished by changing the initial mass fraction of fuel, for example.

The factor $u_p = S_L/U_L$ introduced in Eq. (4) allows to accommodate for the difference between the asymptotic value of laminar flame speed $U_L = \sqrt{2\rho\mathcal{B}\mathcal{D}_T Le\beta^{-2}}\exp\left(-E/2\mathcal{R}T_e\right)$ obtained for large activation energy ($\beta \gg 1$) and the numerical value S_L for finite β. The factor u_p ensures that for a given β the non-dimensional flame speed for a planar adiabatic flame equals one. Of course, the introduction of this factor into the reaction rate is optional. However, it can be convenient for extrapolating the results to different types of fuel by setting as a parameter the value of the planar flame propagation velocity S_L instead of the parameters characterizing the kinetics of complex reactions. The numerical values of u_p were reported in [20] as a function of the Lewis number for $\beta = 10$ and $\gamma = 0.7$. In particular, $u_p \approx 0.942$ for $Le = 1$.

In this work we assume that the thermal conductivity of the solid material is much higher than that of the gas. The temperature of the cylinder remains uniform in this limit being a function of time only. A formal mathematical discussion of this approximation is given in the Appendix. Denoting the temperature of the cylinder as θ_w and the local heat flux on the cylinder surface as $q_L(\varphi) = \partial\theta/\partial r\big|_{r=1}$, the energy balance equation for the cylinder becomes

$$C\frac{d\theta_w}{dt} = q, \quad \text{where} \quad q = \int_0^\pi q_L \, d\varphi \tag{5}$$

is the total heat flux. Here C represents the total dimensionless thermal capacity of the cylinder. In realistic cases of metal holders, for example, this parameter should be much greater than one. However, it is obvious that its value can be easily changed experimentally by layer-by-layer combination of materials with different heat capacity properties, for example.

The boundary conditions for the temperature and mass fraction on the cylinder surface become:

$$0 < \varphi < \pi, \quad r = 1: \quad \theta = \theta_w, \quad \frac{\partial Y}{\partial r} = 0\,. \tag{6}$$

On the x-axis, standard symmetry conditions are assumed:

$$1 < r < \infty, \quad \varphi = 0,\, \pi: \quad \frac{\partial\theta}{\partial\varphi} = \frac{\partial Y}{\partial\varphi} = 0\,. \tag{7}$$

The boundary conditions for the far-field temperature and mass fraction are set as follows:

$$r \to \infty: \quad \begin{cases} \partial^2\theta/\partial r^2 = \partial^2 Y/\partial r^2 = 0\,, & 0 < \varphi < \varphi_*\,. \\ \theta = Y - 1 = 0, & \varphi_* < \varphi < \pi\,, \end{cases} \tag{8}$$

It should be noted that the influence of the far field boundary conditions becomes negligible if the computational domain is chosen large enough. In all calculations presented below we use $\varphi_* = \pi/4$. This value was varied within reasonable limits without any substantial differences in the results.

3 Numerical treatment

The steady Navier-Stokes Eqs. (1) written in terms of the stream function, ψ, and the vorticity, ζ, defined from the relations $v_r = r^{-1}\partial\psi/\partial\varphi$, $v_\varphi = -\partial\psi/\partial r$ and $r\,\zeta = \partial(r\,v_\varphi)/\partial r - \partial v_r/\partial\varphi$, take the form

$$\begin{gathered} \Delta\psi = -\zeta, \quad (\mathbf{v}\cdot\nabla\zeta) = Re^{-1}\Delta\zeta, \\ r=1: \quad \psi = \partial\psi/\partial r = 0; \quad r\to\infty: \quad \psi - r\sin\varphi = \zeta = 0\,. \end{gathered} \tag{9}$$

These equations were solved numerically using a Gauss-Seidel method with over-relaxation where the standard second-order numerical boundary conditions for the vorticity at the cylinder surface were applied, see [21].

Steady as well as time-dependent computations of Eqs. (2)-(3) were carried out in a finite domain, $1 < r < r_{max}$, with the typical value $r_{max} = 10 \div 20$. Changing the domain size within these limits did not lead to noticeable changes in the results for the temperature and mass fraction fields. The main criterion for the accuracy of the calculation was the values of θ_w and q obtained for different sizes of the domain and numerical grid points. All spatial derivatives were discretized using second-order, three-point central finite differences on a rectangular uniform grid with a typical number of grid points $\approx 1000 \times 300$ for Eqs. (2)-(3). Thus, the typical resolution was $\delta r \approx \delta\varphi \approx O(10^{-2})$. The number of grid points was doubled in some cases without significant differences in the results. It should be noted that the calculations of the velocity field are more sensitive to the size of the domain and therefore $r_{max} = 30 \div 50$ was used.

In order to determine steady (but not necessary stable) solutions, the steady counterpart ($\partial/\partial t \equiv 0$) of Eqs. (2)-(3) were solved using a Gauss-Seidel method with over-relaxation. For unsteady calculations an explicit marching procedure was used with first-order discretization in time. The typical time step was $\tau = 10^{-4} \div 10^{-5}$. No significant differences were found in the results when τ was halved.

4 Steady-state solutions

When the flame is stabilized by a bluff-body in a stream, two main mechanisms should be noted. The first consists in the appearance of a zone in which the gas velocity relative to the body is small. Usually this is a recirculation zone within which the gas velocity is directed in the opposite direction with respect to the main flow. The edge of the flame is attached to this zone. This mechanism works regardless of whether the body is adiabatic or cold. It is clear that stabilization may be more difficult in the case of a cold body than in the adiabatic case.

Another mechanism for stabilization is the heating of the body by the flame itself, followed by the conductive heat transfer within the body. In cases when the thermal conductivity of the body is much higher than that of the mixture (this is the case often found in experiments), and at the same time the bluff body does not connect thermally with the outer environment (so that heat losses to the environment are reduced or eliminated), a heat recirculation mechanism is activated. Heat energy is transferred upstream through the body thus preheating the incoming fresh gas ahead. Apparently, both of these mechanisms play an essential role in the situation considered in present study.

4.1 Flow field

It is well known that a recirculation region appears behind the cylinder starting with rather small Reynolds numbers, at $Re \gtrsim 3.5$ in the case of a cold flow. Periodic oscillations in this region appear as Re becomes sufficiently large. As noted in [7], the flow around the cylinder is stabilized in the presence of combustion as compared with the case of cold flow. With confidence, this is due to an increase in the viscosity of the mixture at combustion temperatures. However, the study of this effect is not carried out in our work. As stated above, this work is restricted to cases with relatively small cylinder radii that correspond to $Re < 50$ (based on the cylinder radius). For these values the velocity field remains time-independent even in the case of a cold flow. An example of the velocity field calculated for $Re = 20$ is shown in Fig. 1 in terms of stream function isolines.

4.2 Combustion field

One can see from Eq. (5) that the steady-state solutions ($\partial/\partial t \equiv 0$) satisfy the condition $q = 0$. In these cases, the cylinder temperature, θ_w, should be found as part of the solution and the value of C does not affect it.

We note in parentheses that if the bluff-body has sharp angles, as in [19], the calculation of the total heat flux into the body can meet certain troubles. It can be easily shown that the local heat flux at the surface has a singularity when approaching the corner. Of course, this singularity is integrable (the total flux is finite), but getting the exact value on which the body temperature depends can be difficult.

To find the steady-state solutions corresponding to $q = 0$, the following procedure was used. The steady-state counterpart of Eqs. (2)-(3) was calculated for a fixed cylinder temperature. After that, the value of q given by Eq. (5) was considered as a function of θ_w. The results are shown in Fig. 2 calculated for $Re = 20$ and different values of d. This figure shows that,

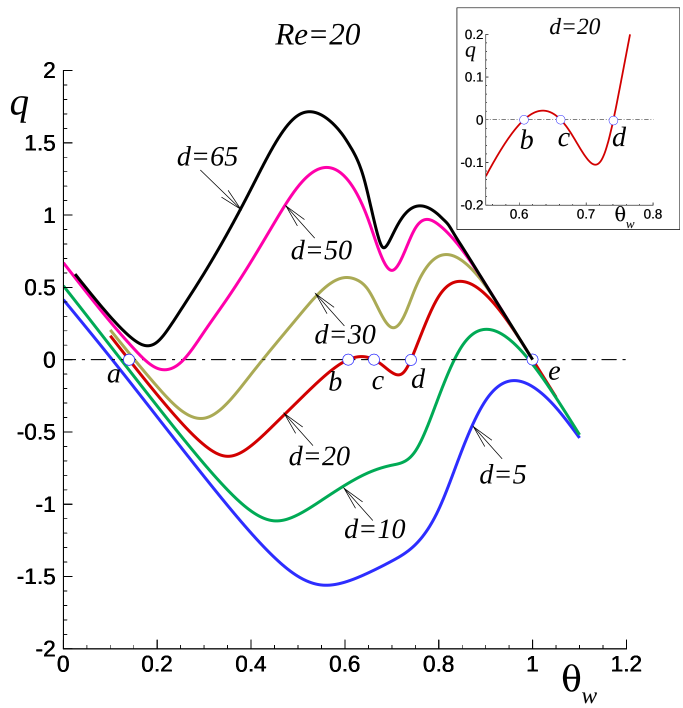

Figure 2: The calculated q values given by Eq. 5 plotted as a function of θ_w for $Re = 20$ and various d. The inset shows the interval of θ_w in which additional roots of the equation $q = 0$ appear.

depending on the Damköhler number, d, the number of roots of the equation $q = 0$ can be higher than one.

Anticipating the description of the steady-state solutions, it should be noted that a stable cold state corresponding to $\theta = 0$ and $Y = 1$ also exists for given values of the parameters. This means that, as one would expect, the flame does not ignite spontaneously and the flame can extinguish under certain conditions.

Figure 2 shows that for relatively small Damköhler numbers the cylinder temperature corresponding to the steady-state condition $q = 0$ is unique and found around $\theta_w \approx 0.15$, as the curve with $d = 5$ shows. For larger values of d, two additional states appear illustrated by the curve with $d = 10$. One state has an intermediate cylinder temperature, while for the other the cylinder temperature is close to adiabatic $\theta_w \approx 1$. For $Re = 20$, the emergence of these two states occurs at $d \gtrsim 7.05$.

It is interesting to note that with a further increase in d, two additional roots of the equation

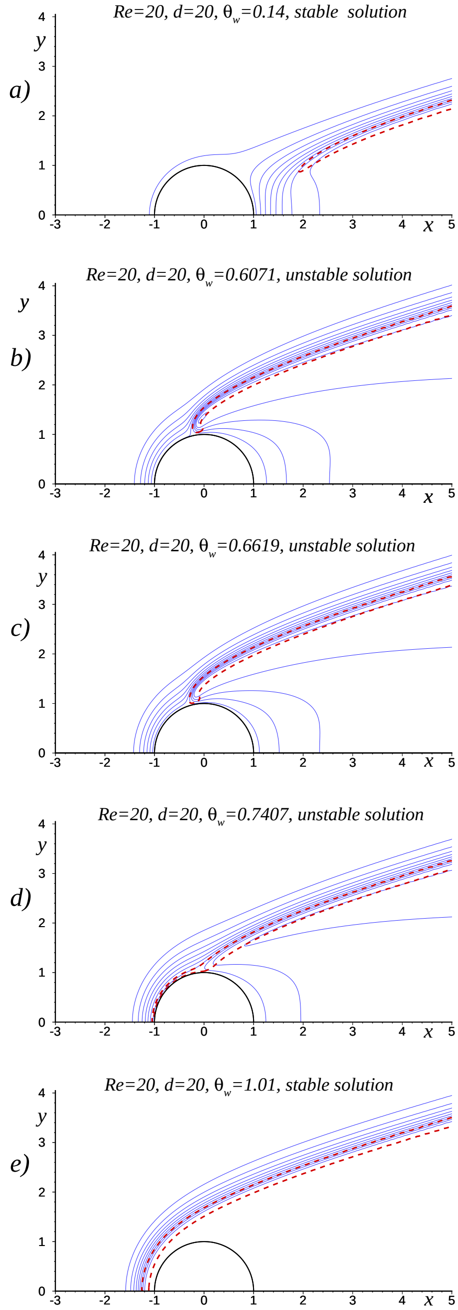

Figure 3: Temperature distributions (solid lines, in an interval 0.1) and the reaction rate isoline (a dashed line, plotted for $\omega = 10$) for various steady-state solutions marked with open circles "a", "b", "c", "d" and "e" in Fig. 2, for $Re = 20$ and $d = 20$.

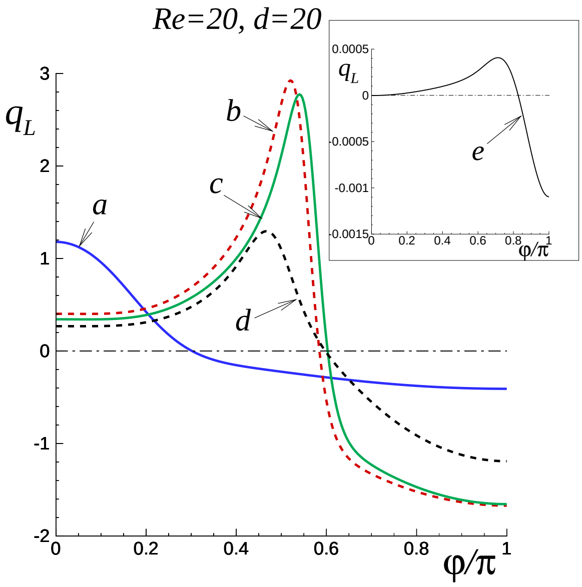

Figure 4: Local heat flux distribution on the cylinder surface calculated for various solutions marked with open circles in Fig. 2. The flux for the "e" solution is given in the inset.

$q = 0$ appear. This effect is illustrated by the curve with $d = 20$ and occurs approximately in the interval $19.6 \lesssim d \lesssim 23.2$ (for $Re = 20$). Thus, there are five steady-state solutions in this interval of the Damköhler number. These solutions are indicated by open circles and the letters "a, b, c, d, e" in Fig. 2. These additional roots then disappear for $d \gtrsim 23.2$.

Figure 2 shows that with a further increase in d, the steady-state with a relatively cold cylinder disappears and the only stationary state is that with the cylinder temperature close to adiabatic. This happens when $d \gtrsim 56.3$. It is obvious that all the critical values of the Damköhler number given here depend on other parameters, in particular, on the Reynolds number.

The flame structure for different values of the Damkohler number is illustrated in Fig. 3 for $d = 20$. Temperature contours (solid lines) are given in the interval $\delta\theta = 0.1$. Dotted lines in all figures denote the isoline of the reaction rate $\omega = 10$. The solution corresponding to point "a" in Fig. 2 is characterized by a relatively cold cylinder temperature and a flame located behind the cylinder. For solution "e", for which the temperature of the cylinder is very close to the adiabatic temperature, the flame originates in front of the cylinder and surrounds it. For other solutions, intermediate configurations are found.

The local heat flux $q_L = \partial\theta/\partial r|_{r=1}$ on the surface of the cylinder is shown in Fig. 4 as a function of φ. Note that $\varphi = 0$ corresponds to the rear point of the cylinder. It can be seen that

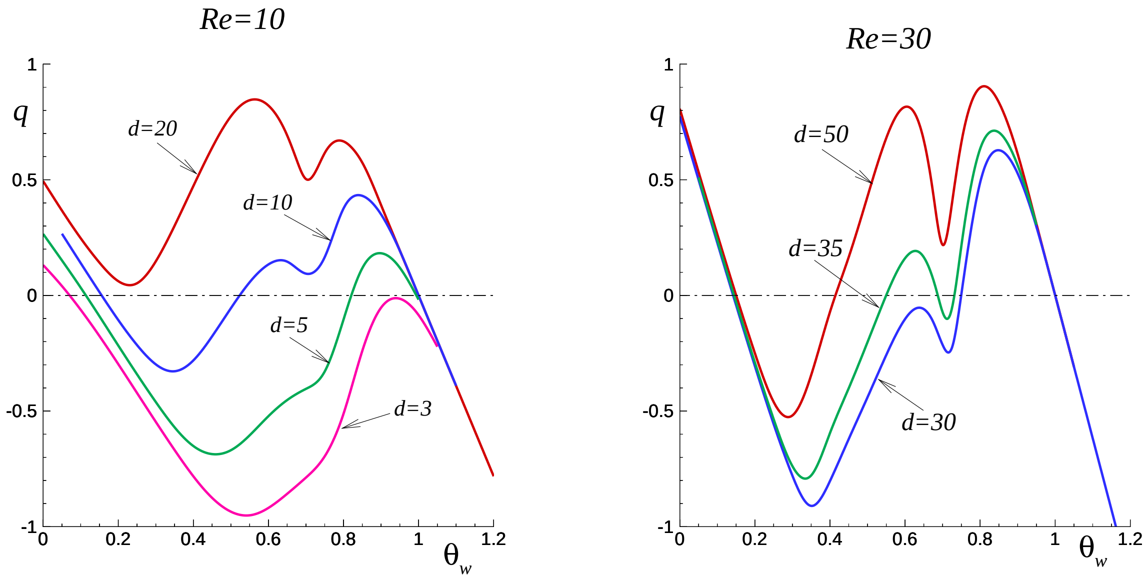

Figure 5: The calculated q values given by Eq. 5 as a function of θ_w for $Re = 10$ (left plot) and $Re = 30$ (right plot) and various d.

for all solutions "a"-"e" the cylinder is heated ($q_L > 0$) through its rear and cooled ($q_L < 0$) through the front part. It is noticeable that the heat flux q_L is very small for the "e" solution compared to other solutions.

The dependence of the total heat flux on the cylinder temperature for other Reynolds numbers is qualitatively similar to those shown in Fig. 2. For $Re = 10$ and $Re = 30$, these dependencies are shown in Fig. 5 for different Damköhler numbers. This indicates that the effect of multiplicity of steady-state solutions for a flame in a certain range of Damköhler numbers is robust enough for a change in the Reynolds number. It can be noted that the Damköhler and Reynolds numbers enter into Eqs. (2)-(3) as d/Re. On the other hand, an increase in the Reynolds number affects only the length of the recirculation zone, leaving the flow structure almost unchanged. This indicates that the dependence of the critical Damköhler numbers between which the multiplicity of steady-state solutions takes place on the Reynolds number should be close to linear. The approximate minimum and maximum critical Damköhler numbers are presented in Fig. 6 as functions of the Reynolds number.

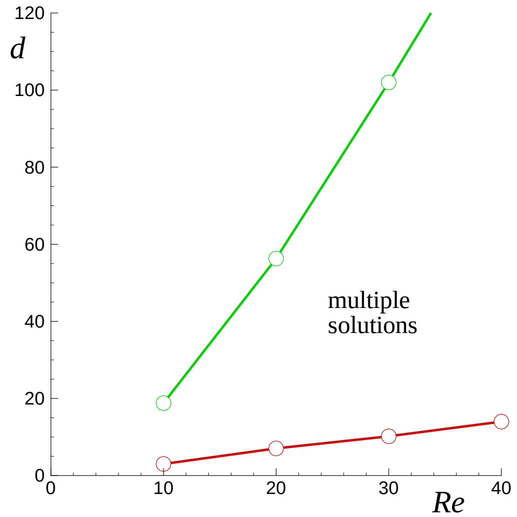

Figure 6: Dependence of the maximum and minimum critical Damköhler numbers between which the multiplicity of steady-state solutions takes place on the Reynolds number.

5 Stability and time-dependent dynamics

In order to check the above steady-state solutions for stability, time-dependent Eqs. (2)-(3) and (5) were calculated for different values of the parameter C. First, the temperature and mass fraction distributions obtained for solutions "b", "c", and "d" were chosen as initial conditions. The time histories of θ_w are shown in Fig. 7.

First of all it should be noted that the accuracy of calculating the steady-state solutions taken as initial conditions was high, but finite. It can be seen in Fig. 7 that changes in the value of θ_w for all three initial distributions "b", "c" and "d"" are negligible at the initial stage of calculations, $0 < t \lesssim 10$. Obviously, the duration of this time interval depends on the accuracy of calculating the initial steady-state distributions. If we assume a hypothetical ideal case of a numerical procedure with infinitely high accuracy, the duration of this initial interval (with zero values of time derivatives) would be infinite as well. Therefore in the ideal case, for the development of dynamics, it is necessary to introduce small, but not zero, perturbations, even if the solution is unstable.

After passing this interval, the small disturbances gradually increase and changes in θ_w become visible. Finally, the solution approaches one of the states "a" or "e". The oscillatory

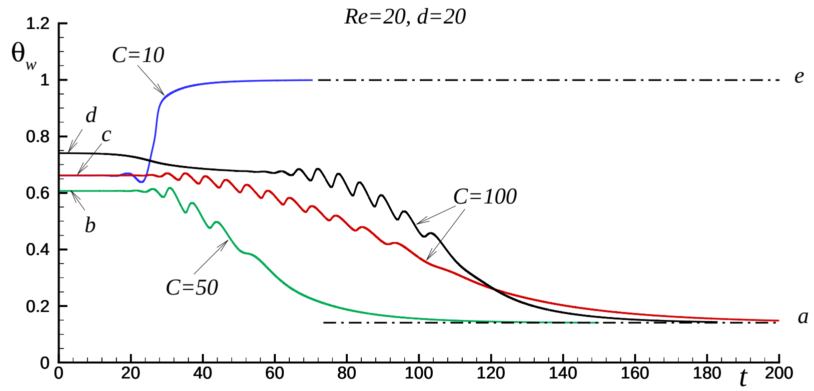

Figure 7: Time histories of cylinder temperature calculated for $Re = 20$, $d = 20$ and various values of C. Steady-state distributions "b", "c", and "d" were chosen as the initial distributions for temperature and mass fraction. Dash-dotted lines indicate temperatures for stable states "a" and "e".

nature of the transitional dynamics should also be noted. Interestingly, the transition to states "a" or "e" is affected by the values of parameter C. Thus, the numerical simulations show that states "b", "c", and "d" are unstable, while states "a" and "e" are stable. This is indicated in Fig. 3.

The simulation results presented in Fig. 7 are especially unexpected for the "c" mode. Indeed, when analyzing the response curve shown in Fig. 2 it may seem that the steady-state "c" should be stable. According to Fig. 2 (see the inset), with a random small increase in the temperature of the cylinder, θ_w, the heat flux q to the cylinder becomes negative and the cylinder should seem to be cooled. Equivalently, after an occasional small cooling of the cylinder, it should be heated (q becomes positive). However, Fig. 7 shows that such qualitative reasoning does not work for the steady-state "c" which is apparently unstable. In this regard, it should be noted that a rigorous analysis of the stability of one or another steady-state solution to small perturbations should be performed by solving a much more complex eigenvalue problem than a qualitative evaluation of a steady-state response curve. The heat flux, q, is not a function of one argument, θ_w, but is the result of integrating the temperature field outside the cylinder. This issue remains outside the scope of this article, where conclusions about stability are made on the basis of time dependent simulations. The numerical simulations starting from the steady-state "c" solution were carried out up to $C = 500$ with the same result: the initial small perturbations due to the

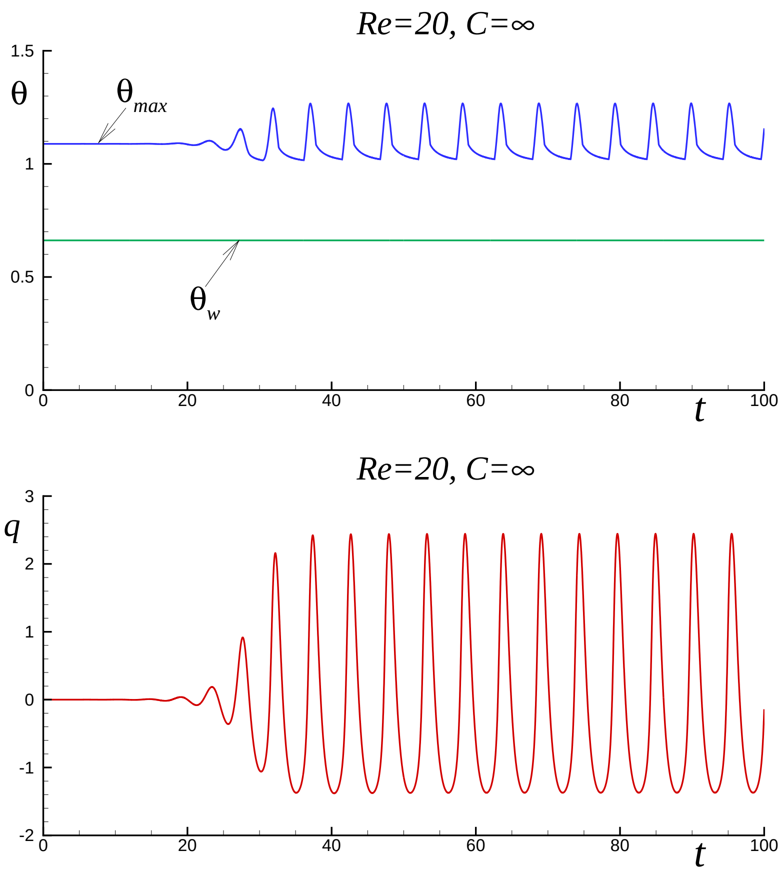

Figure 8: Time history of the maximum temperature in the domain , θ_{max} (upper plot), and the heat flux, q (lower plot), calculated in the limit $C \to \infty$ with $\theta_w = 0.6619$ corresponding to the "c" steady-state solution.

finite accuracy of the numerical code always increased leading to a transition to another mode.

In order to clarify more this effect of the "c" mode instability, the following numerical simulation was carried out. As in the previous time-dependent calculations, the steady-state solution obtained by the Gauss-Seidel method and by setting $\partial/\partial t = 0$ in Eq. (2)-(3) was used as an initial condition. If we formally impose $C \to \infty$ (infinitely large thermal capacity of the cylinder), then θ_w will not change according to Eq. (5). Figure 8 shows the result of this calculation, where the maximum temperature in the domain, θ_{max}, and the heat flux, q, are given as functions of time. It can be seen that at fixed $\theta_w = 0.6619$ corresponding to the "c" steady-state solution, the flame suffers oscillatory dynamics, which is in no way related to changes in the cylinder temperature. It can be seen that the amplitude of the heat flux oscillations significantly exceeds

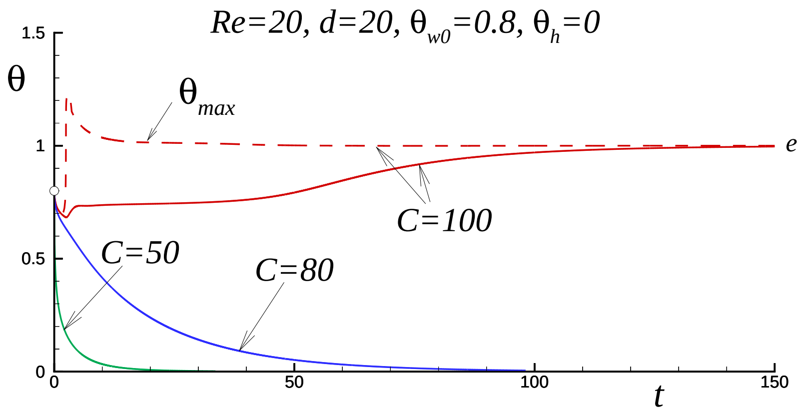

Figure 9: Time histories of cylinder temperature calculated for $Re = 20$, $d = 20$ and various values of C, all curves for $\theta_h = 0$; a dashed line shows the maximum temperature in the domain for $C = 100$.

the values of the local steady-state maximum and minimum of q visible in the response curve (see Fig. 2) in the vicinity of the "c" solution. From this we can conclude that at finite values of C, this intrinsic flame instability eventually leads to destabilization of the "c" steady-state with the subsequent transition to another, now already stable, regime. The characteristic time scale of cylinder temperature changes is of the order of C. Obviously, the effect described here cannot be explained from the qualitative analysis of the steady-state response curve.

Although the appearance of oscillatory behavior for premixed flames with $Le = 1$ does not happen very often, it is possible that the phenomenon described above is of a similar nature to that of the flame dynamics reported in [22, 23]. In these studies, oscillatory flames with unity Lewis number were also described as being caused by a heated surface. Anyway, the particular question regarding the stability of the "c" mode, interesting from a stability point of view, is of little practical importance, since this situation corresponds to a rather narrow range of d parameters. Outside this interval, the only intermediate state appearing between the stable cold and stable hot regimes, if it exists, is definitely unstable.

Numerical simulations were also carried out using the following initial distributions applied at $t = 0$:

$$\theta = \left\{ \begin{array}{ll} \theta_{w0}, & r = 1 \\ 0, & r > 1 \end{array} \right\} + \theta_h \exp\{-[(x - x_*)^2 + y^2]/r_*^2\}, \quad Y = 1\,. \tag{10}$$

The first term in Eq. (10) corresponds to an instantaneous initial heating of the cylinder to temperature θ_{w0}. The second term describes an initial hot spot with temperature θ_h and radius r_*

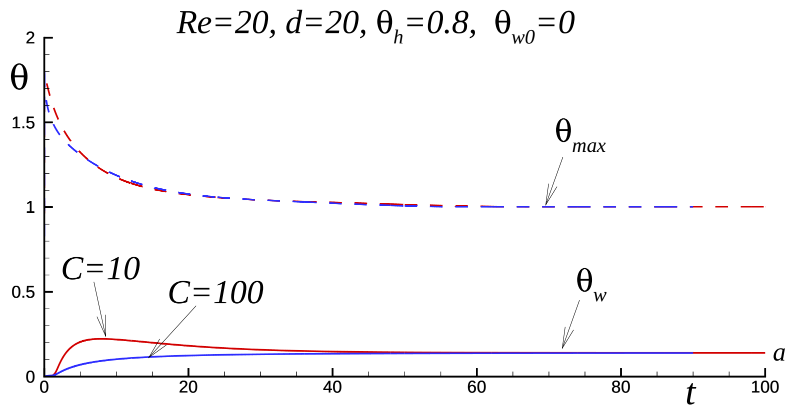

Figure 10: Time histories of cylinder temperature calculated for $Re = 20$, $d = 20$ and various values of C, all curves for $\theta_{w0} = 0$; dashed lines show the maximum temperature in the domain.

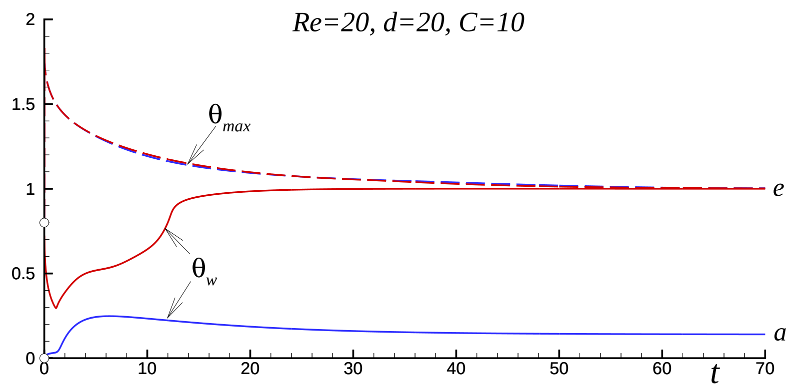

Figure 11: Time histories of cylinder temperature, θ_w, and the maximum temperature in the domain, θ_{max}, calculated for $Re = 20$, $d = 20$ and $C = 10$. Open circles indicate the initial cylinder temperature.

located on the $x = x_*$ point at the axis $y = 0$. Numerical values were chosen as $r_* = 1$ and $x_* = 3$. These two terms were applied both separately and simultaneously.

Let us first consider the flame dynamics when only the cylinder is initially heated, namely $\theta_h = 0$ is applied in Eq. (10). Figure 9 shows with solid lines the time histories of the cylinder temperature for various values of C when its initial temperature was chosen equal to $\theta_{w0} = 0.8$. This value is indicated by an open circle on the figure. All cases were calculated for $Re = 20$ and $d = 20$. It can be seen that at relatively low C the flame is not established and the final state of the system is the trivial cold state. However, at $C = 100$, the flame is established in a state that corresponds to the state "e" in Fig. 3. We also show in Fig. 9 with a dotted line the evolution of the maximum temperature in the domain for $C = 100$. It should be noted that when only the cylinder is heated in the initial temperature distribution (that is, $\theta_h = 0$), the final state is the stable state "e" at sufficiently high C, and never the state "a" which is also stable.

The flame dynamics becomes different if the cylinder is not heated initially ($\theta_{w0} = 0$) but a hot spot is applied. Figure 10 shows the dynamics of the flame in this case with the hot spot initial temperature $\theta_h = 0.8$ and two values of C. The solid curves give the time histories of θ_w, and the dashed curves show the maximum temperature in the domain, θ_{max}. It can be seen that in both cases the final state of the cylinder is the state "a", that is, a stable state with a relatively cold cylinder temperature.

Obviously, with the help of the initial heating of the cylinder, it is possible to control the final convergence to one or another stable state. Figure 11 shows the cases with $\theta_h = 0.8$ (the hot spot is applied) and two different initial cylinder temperatures, $\theta_w = 0$ and 0.8, indicated in the figure with open circles. All curves calculated for $Re = 20$, $d = 20$ and $C = 10$. For $\theta_{w0} = 0$, the system approaches the mode "a" corresponding to the relatively cold cylinder temperature, $\theta_w \approx 0.14$, while for $\theta_{w0} = 0.8$ the final steady-state is the mode "e" with $\theta_w \approx 1$. We also show the dependence of the maximum temperature in the domain for the two cases using the dashed curves which practically coincide in both cases. These examples demonstrate once again that there are two stable steady-state flames corresponding to two different cylinder temperatures in addition to the frozen steady-state solution.

6 Summary and discussion

In present work, the study of flame stabilization by a bluff body, a cylinder, placed perpendicularly in a homogeneous flow of a combustible mixture is carried out. We have used some simplifying assumptions in the formulation. The main simplifications are the application of the diffusion-thermal model in which the density changes are neglected and the assumption that the thermal conductivity of the cylinder material is much higher than that of the mixture around. The use of these simplifications made possible to understand the physics of the phenomenon through low-cost computations. It should be noted that the first, diffusion-thermal, assumption is widely used in combustion giving qualitatively correct results. The second simplification of a large ratio of the thermal conductivities is not too restrictive. To avoid computational difficulties, the problem is considered for relatively low Reynolds numbers when self-excited oscillations in the gas velocity field do not arise.

An important difference from many other studies on flame stabilization is the requirement that the cylinder is thermally insulated from other bodies, being in thermal contact only with the gas. In this case, the temperature of the cylinder cannot be fixed, and the mutual thermal interaction between the cylinder material and the surrounding mixture should be allowed. Physically realistic steady-states are those at which the total heat flux on the cylinder surface is zero. This condition determines the temperature of the cylinder.

A numerical study of the problem showed that at a fixed velocity of the incident flow, there is an interval of combustion reaction intensity (controlled by the Damköhler number) within which the problem has multiple steady-state solutions. The total number of different non-trivial steady-states, that is, solutions involving combustion, can reach five. It is necessary to add to this number a trivial (cold) steady state without flame. Outside of this interval of Damköhler numbers, within which there is a multiplicity of solutions, only one nontrivial steady-state solution remains.

As the time-dependent simulations showed, not all the solutions are stable. However, summarizing the results of the numerical analysis, it turned out that at least two stationary states are stable. For the first steady solution, the flame spreads out behind the cylinder and its temperature is relatively low. For the other stable solution, the cylinder is heated to a high temperature close to the adiabatic temperature of the mixture and the flame is located also around the cylinder. It was shown by means of numerical simulations that by choosing certain initial conditions for the flame initiation it is possible to ensure the establishment of one or the other of the stable modes. Once again, we want to note that the resulting effect, the multiplicity of stationary states, can be observed only in a certain interval of Damköhler numbers.

It is important to mention that the estimate of the dimensional radius of the cylinder corresponding to the characteristic dimensionless parameters used in this study gives $R = 0.1 \div 3\, mm$ for $U = 1\, m/s$ and $Re = \rho U R/\mu = 20$. Decreasing the flow velocity leads to even larger values for the dimensional radius at a fixed Reynolds number. The resulting interval for R depends on the temperature at which the viscosity μ is estimated. It would be natural to assume that the viscosity assessment should be made at a temperature close to the adiabatic temperature observed in the flame zone. In this case, the upper limit for the radius estimate takes place. If this is the case, then the estimate for the reduced Damköhler parameter turns out to be of the order of $d = R^2/\delta_T^2 = 20 \div 40$, if we take the thermal width of the flame, δ_T, of the order of a fraction of millimeter.

Finally, the authors want to note that although the problem requires further research, in which the assumptions of the original model should be weakened (for example, by including the thermal expansion of the mixture), the results obtained are mainly related to the effect of heat recirculation inside a solid body. Namely, the heat energy is transferred upstream through the solid phase thus heating the incoming mixture. It is hoped that taking thermal expansion into account will only lead to a shift in the critical parameters at which the emergence of the multiplicity phenomenon occurs.

Acknowledgement

This work was financed by project #PID2019-108592RB-C42 / AEI / 10.13039/501100011033.

Appendix. Highly conductive body limit

While this limit can be considered intuitively, a brief mathematical discussion is also helpful. Consider the transfer of heat inside the cylinder; and index w denotes below the properties related to it. Using the same scales as in Eqs. (2)-(3), the following dimensionless equation can be written

$$\mu \frac{\partial \theta_w}{\partial t} = \frac{\Lambda}{Re\,Pr}\,\Delta\theta_w, \quad \Lambda \frac{\partial \theta_w}{\partial r}\bigg|_{r=1} = \frac{\partial \theta}{\partial r}\bigg|_{r=1}, \tag{A1}$$

where θ_w denotes here the spatial distribution of temperature inside the cylinder. Two additional dimensionless parameters appear: the thermal conductivity ratio, $\Lambda = \lambda_w/\lambda$, relating the solid material conductivity λ_w to the gas conductivity λ, and the parameter $\mu = \rho_w c_w/\rho c_p$ representing the ratio of thermal capacities per unit volume.

Consider the limit of $\Lambda \gg 1$. Assuming (formally) that all remaining parameters are of order unity, we expand θ_w in the form $\theta_w = \theta_w^{(0)} + \Lambda^{-1}\theta_w^{(1)} + \dots$. To the leading order, Eqs. (A1) are reduced to

$$\Delta\theta_w^{(0)} = 0, \quad \partial\theta_w^{(0)}/\partial r|_{r=1} = 0\,.$$

Obviously, $\theta_w^{(0)}$ can be a function of time, only.

We now proceed to the next order in Λ^{-1}. The corresponding equations are reduced to

$$\mu \frac{d\theta_w^0}{dt} = \frac{1}{Re\,Pr}\,\Delta\theta_w^{(1)}, \quad \frac{\partial \theta_w^{(1)}}{\partial r}\bigg|_{r=1} = \frac{\partial \theta}{\partial r}\bigg|_{r=1}.$$

After integration over the cylinder volume and dropping the superscript, Stokes' theorem leads to Eq. (5), where $C = \pi\mu Re\, Pr/2$.

References

[1] F.H. Wright, Some aerodynamics factors influencing bluff body flame stabilization, *Combust. Flame* 2 (1958) 96-97.

[2] F.H. Wright, Bluff-body flame stabilization - blockage effects, *Combust. Flame* 3 (1959) 319-337.

[3] T. Maxworthy, On the mechanism of bluff body flame stabilization at low velocities, *Combust. Flame* 6 (1962) 233-244.

[4] K.M. Kundu, D. Banerjee, D. Bhaduri, Theoretical analysis on flame stabilization by a bluff-body, *Combust. Sci. Tech.* 17 (1977) 153-162.

[5] K.M. Kundu, D. Banerjee, D. Bhaduri, On flame stabilization by bluff-bodies, *J. Eng. Power* 102 (1980) 209-214.

[6] A. Fan, J. Wan, K. Maruta, H. Yao, W. Liu, Interactions between heat transfer, flow field and flame stabilization in a micro-combustor with a bluff body, *Int. J. Heat Mass Trans.* 66 (2013) 72-79.

[7] M. Miguel-Brebion, D. Mejia, P. Xavier, F. Duchaine, B. Bedat, L. Selle, T. Poinsot, Joint experimental and numerical study of the influence of flame holder temperature on the stabilization of a laminar methane flame on a cylinder, *Combust. Flame* 172 (2016) 153-161.

[8] K. Kedia, C. Safta, J. Ray, H. Najm, A. Ghoniem, A second-order coupled immersed boundary-SAMR construction for chemically reacting flow over a heat-conducting Cartesian grid-conforming solid, *J. Comput. Phys.* 272 (2014) 408-428.

[9] K. Kedia, A. Ghoniem, The anchoring mechanism of a bluff-body stabilized laminar premixed flame, *Combust. Flame* 161 (2014) 327-339.

[10] K.S. Kedia, A.F. Ghoniem, The blow-off mechanism of bluff-body stabilized laminar premixed flame, *Combust. Flame* 162 (2015) 1304-1315.

[11] K.S. Kedia, A.F. Ghoniem, The response of a hamonically forced premixed flame stabilized on a heatconducting bluff-body, *Combust. Flame* 35 (2015) 1065-1072.

[12] P. Xavier, A. Ghani, D. Mejia, M. Miguel-Brebion, M. Bauerheim, L. Selle, T. Poinsot, Experimental and numerical investigation of flames stabilised behind rotating cylinders: interaction of fames with a moving wall, *J. Fluid Mech.* 813 (2017) 127-151.

[13] D. Mejia, M. Bauerheim, P. Xavier, B. Ferret, L. Selle, T. Poinsot, Stabilization of a premixed laminar flame on a rotating cylinder, *Proc. Combust. Inst.* 36 (2017) 1447-1455.

[14] D. Mejia, M. Miguel-Brebion, A. Ghani, T. Kaiser, F. Duchaine, L. Selle, T. Poinsot, Influence of flame-holder temperature on the acoustic flame transfer functions of a laminar flame, *Combust. Flame* 188 (2018) 5-12.

[15] C. Jiménez, D. Michaels, A. Ghoniem, Stabilization of ultra-lean hydrogen enriched inverted flames behind a bluff-body and the phenomenon of anomalous blow-off, *Combust. Flame* 191 (2018) 86-98.

[16] C. Jiménez, D. Michaels, A. Ghoniem, Ultra-lean hydrogen-enriched oscillating flames behind a heat conducting bluff-body: Anomalous and normal blowoff, *Proc. Combust. Ins.* 37 (2019) 1843-1850.

[17] Y.Yan, Z. He, Q. Xu, L. Zhang, L. Li, Zh. Yang, J. Ran, Numerical study on premixed hydrogen/air combustion characteristics in microcombustor with slits on both sides of the bluff body, *Int. J. Hydr. Eng.* 44 (1919) 1998-2012.

[18] V.N. Kurdyumov, Y.L. Shoshin, L.P.H. de Goey, Structure and stability of premixed flames stabilized behind the trailing edge of a cylindrical rod at low Lewis numbers, *Proc. Combust. Ins.* 35 (2015) 981-988.

[19] S. Berger, F. Duchaine, L.Y.M. Gicquel, Bluff-body thermal property and initial state effects on a laminar premixed flame anchoring pattern, *Flow Turb. Combust.* 100 (2018) 561-591.

[20] V.N. Kurdyumov, Lewis number effect on the propagation of premixed flames in narrow adiabatic channels: Symmetric and non-symmetric flames and their linear stability analysis, *Combust. Flame* 158 (2011) 1307-1317.

[21] C.A.J. Fletcher, Computational technics for fluid dynamincs, Springer-Verlag 1988.

[22] V.N. Kurdyumov, J.-M. Truffaut., J. Quinard, A. Wangher, G. Searby, Oscillations of premixed flame in tubes near the flashback conditions, *Combust. Sci. Tech.* 180 (2008) 731-742.

[23] V.N. Kurdyumov, G. Pizza, C.E. Frouzakis, J. Mantzaras, Dynamics of premixed flames in a narrow channel with a step-wise wall temperature, *Combust. Flame* 156 (2009) 2190-2200.